Publishing Excellence Inspiring Progress
ARISTON PUBLICATIONS
MatSci Express
ISSN: 2997-8440 www.aristonpubs.com/matsci-express https://doi.org/10.69626/mse.2025.0192

RESEARCH ARTICLE

Enhanced Acetone Sensing Performance of Silver–Doped Tin Oxide ($Sn_{1-x}Ag_xO$) Thick Films Synthesized via Hydrothermal Method

Laxman P. Chikhale *, Nitin A. Tupsaminar

ABSTRACT: Pure and silver-doped tin oxide (SnO_2) nanostructured powders were synthesized using a hydrothermal method, followed by the fabrication of gas sensor elements via screen-printing technique. The structural and morphological properties of the synthesized materials were characterized using X-ray diffraction (XRD), confirming the formation of a hexagonal wurtzite structure with an average crystallite size ranging between 60–100 nm. The gas sensing performance of the undoped and Ag-doped SnO_2 thick films was systematically evaluated for acetone detection at varying operating temperatures (200–450°C). The results demonstrated that Ag-doped SnO_2 sensors exhibited significantly enhanced sensitivity toward acetone at an optimal operating temperature of 350°C compared to their undoped counterparts. The sensor with 1 mol% Ag doping (S2) displayed the highest response (94%) toward 2000 ppm acetone, along with rapid response and recovery times of 14 seconds and 30 seconds, respectively. Additionally, the Ag-doped sensor exhibited excellent selectivity for acetone over other interfering gases such as ethanol, LPG, and NH_3. Stability tests conducted over two months confirmed the long-term reliability of the sensor, with only a marginal decrease in performance. The improved sensing characteristics were attributed to the catalytic effect of silver doping, which facilitates oxygen adsorption and enhances surface reactions with acetone molecules. These findings highlight the potential of Ag-doped SnO_2 nanostructures as high-performance gas sensors for industrial safety and medical diagnostics, particularly in non-invasive diabetes monitoring through breath acetone detection.

Keywords: SnO_2 gas sensor, Silver doping, Hydrothermal synthesis, Acetone detection, Screen-printing technique, Selective gas sensing.

Received: 02 January 2024; Revised: 19 February 2025; Accepted: 27 February 2025; Published Online: 23 March 2025

1. INTRODUCTION

In recent years, the development of nanostructured gas sensors has garnered significant attention due to their critical role in detecting toxic and hazardous gases in industrial, environmental, and medical applications. The increasing need for real-time monitoring of air quality and industrial emissions has driven research into advanced sensing materials capable of high sensitivity, selectivity, and stability. Among various sensing technologies, metal oxide semiconductor (MOS)-based gas sensors have emerged as a leading solution due to their excellent electrical properties, tunable surface chemistry, and cost-effective fabrication processes [1]. Commonly studied MOS materials include tin oxide (SnO_2), tungsten oxide (WO_3), and titanium dioxide (TiO_2), each offering distinct advantages depending on the target gas and operating conditions [2].

Tin oxide (SnO_2), an n-type II-VI semiconductor with a direct bandgap of 3.36 eV at room temperature, has been extensively investigated for gas sensing applications owing to its high electron mobility, thermal stability, and surface reactivity [3]. The gas sensing mechanism in SnO_2 relies on changes in electrical resistance due to surface interactions between adsorbed oxygen species and target gas molecules. However, pure SnO_2 sensors often suffer from limitations

Department of Physics, Venkatesh Mahajan Senior College, Dharashiv, District-Dharashiv, Maharastra 413501, India.

* Author to whom correspondence should be addressed: laxmanchikhale@gmail.com (Laxman P. Chikhale)

such as poor selectivity, high operating temperatures, and slow response/recovery kinetics. To overcome these challenges, researchers have explored doping SnO_2 with various transition and noble metals, including aluminum (Al), copper (Cu), and palladium (Pd), which modify the electronic structure and catalytic properties of the material [4]. While these dopants enhance sensor performance, issues such as synthesis complexity, dopant agglomeration, and long-term stability remain critical challenges that hinder large-scale deployment [5].

The hydrothermal synthesis method has gained prominence as a versatile and scalable technique for producing high-purity metal oxide nanostructures with controlled morphology and crystallinity [6-9]. Unlike conventional solid-state or sol-gel methods, hydrothermal synthesis allows for precise tuning of particle size, shape, and doping concentration under relatively mild conditions, resulting in materials with enhanced surface area and defect chemistry [6]. This method is particularly advantageous for gas sensor applications, as it enables the production of nanostructures with high surface-to-volume ratios, facilitating efficient gas adsorption and charge transfer processes. Additionally, the environmentally benign nature of hydrothermal synthesis makes it a sustainable alternative for large-scale sensor fabrication [7-11].

Acetone, a volatile organic compound (VOC) widely used in industrial processes such as plastic manufacturing, pharmaceutical production, and laboratory solvents, poses significant health risks upon prolonged exposure. Inhalation of acetone vapors can lead to respiratory irritation, central nervous system depression, and damage to internal organs such as the liver and kidneys [8]. Beyond industrial safety concerns, acetone is also a crucial biomarker in human breath, with elevated concentrations ($\geq$ 1.8 ppm) strongly correlated with diabetes mellitus. Non-invasive breath acetone detection has thus emerged as a promising diagnostic tool for diabetes monitoring, eliminating the need for invasive blood tests [9]. However, the development of reliable acetone sensors requires overcoming challenges such as interference from other VOCs (e.g., ethanol, methanol) and maintaining stable performance under varying humidity and temperature conditions [10-14].

In this study, we address these challenges by synthesizing pure and silver (Ag)-doped SnO_2 nanostructures via a hydrothermal method and fabricating thick-film gas sensors using a screen-printing technique. Silver was selected as a dopant due to its excellent catalytic activity, which enhances the surface reactivity of SnO_2 toward acetone molecules while improving charge carrier mobility. The incorporation of Ag into the SnO_2 lattice was systematically characterized using X-ray diffraction (XRD), confirming the formation of a hexagonal wurtzite structure with controlled crystallite sizes. Gas sensing evaluations demonstrated that Ag-doped SnO_2 sensors exhibit superior acetone sensitivity (94% response to 2000 ppm) at an optimal operating temperature of 350°C, along with rapid response (14s) and recovery (30 s) times. Furthermore, the sensors displayed exceptional selectivity for acetone over interfering gases such as ethanol and LPG, as well as long-term stability over a two-month testing period.

The key novelty of this research lies in the optimized hydrothermal synthesis of Ag-doped SnO_2 nanostructures, which achieves a balance between high sensitivity and selectivity for acetone detection. Unlike previous studies focusing on Pd or Cu doping, this work demonstrates that Ag doping significantly enhances sensor performance while maintaining cost-effectiveness and scalability. The screen-printed thick-film fabrication method further ensures practical applicability for industrial and medical sensing devices. Additionally, the study provides a detailed mechanistic understanding of the role of Ag in promoting oxygen chemisorption and surface reactions with acetone, contributing to the broader field of MOS-based gas sensors. These advancements position Ag-doped SnO_2 as a promising candidate for next-generation acetone sensors in both industrial safety and diabetes diagnostics.

2. EXPERIMENTAL DETAILS

2.1. Materials Synthesis

The synthesis of pure and silver-doped tin oxide ($Sn_{1-x}Ag_xO$) powders was carried out using a hydrothermal method. High-purity analytical grade precursors were employed, including tin(II) acetate dihydrate ($Sn(CH_3COO)_2 \cdot 2H_2O$, silver nitrate hexahydrate ($AgNO_3 \cdot 6H_2O$), and sodium hydroxide (NaOH, 99.9% purity), all used as received without further purification. For the preparation of Ag-doped SnO_2, stoichiometric amounts of tin acetate (0.1 M) and silver nitrate (1.6 mmol) were dissolved in 160 mL of deionized water under continuous magnetic stirring. The pH of the solution was carefully adjusted to 10 by dropwise addition of 1 M NaOH solution, resulting in the formation of a homogeneous suspension. This mixture was subsequently transferred to a 200 mL Teflon-lined stainless steel autoclave and maintained at 95°C for 3 hours to facilitate the hydrothermal reaction. After natural cooling to room temperature, the resulting precipitate was collected by centrifugation at 8000 rpm for 10 minutes and subjected to three consecutive washing cycles with deionized water to remove residual ions. The purified product was then dried in air at 50°C for 2 hours to obtain the final powder. Pure SnO_2 was synthesized following an identical protocol, omitting the addition of silver nitrate. The prepared samples were designated as S1 (pure SnO_2), S2 (1 mol% Ag-doped SnO_2), and S3 (10 mol% Ag-doped SnO_2), with corresponding crystallite sizes of 68 nm, 55 nm, and 62 nm, respectively, as determined by X-ray diffraction analysis. Table 1 exhibits the details of the samples.

2.2. Structural Characterization

The crystalline structure and phase purity of the synthesized

powders were characterized using X-ray diffraction (XRD, Bruker D8 Advance) with Cu Kα radiation (λ = 1.5406 Å) ope.ing at 40 kV and 40 mA. Diffraction patterns were recorded in the 2θ range of 20-80° with a step size of 0.02° and a counting time of 1 s per step. The average crystallite size was calculated using the Scherrer equation applied to the most intense diffraction peaks, while lattice parameters were refined using Rietveld analysis. The presence of secondary phases and the effect of Ag doping on the crystal structure were carefully examined through peak position shifts and relative intensity variations in the diffraction patterns.

Table 1. Sample identification for the prepared Sn_{1-X} Ag_XO nanomaterials.

Mol. % Ag doping	Sample Code	Crystal size
Pure SnO_2	S1	68
X=0.01	S2	55
X=0.10	S3	62

2.3. Sensor Fabrication

Thick film gas sensors were fabricated using a screen-printing technique on pre-cleaned alumina substrates (96% purity, 5 × 5 mm²). The synthesized powders were mixed with an organic vehicle (α-terpineol and ethyl cellulose) to form a printable paste with appropriate viscosity. This paste was then deposited onto the substrates through a 325-mesh stainless steel screen, followed by drying at 120°C for 30 minutes to remove organic solvents. The printed films were subsequently sintered in a programmable furnace at 700°C for 2 hours in air to ensure proper adhesion and electrical continuity. Interdigitated silver electrodes (thickness ≈ 10 µm) were patterned on the sintered films using a shadow mask and thermal evaporation technique, providing ohmic contacts for electrical measurements. The final sensor devices were aged at 300°C for 24 hours in air to stabilize their sensing properties prior to gas testing.

2.4. Gas Sensing Measurements

The gas sensing properties were evaluated using a custom-built static gas sensing system equipped with a temperature-controlled chamber and precision mass flow controllers. The sensor response was measured as the relative change in resistance (R_a/Rg) when exposed to target gases, where R_a and Rg represent the sensor resistance in air and in the presence of test gas, respectively. Acetone vapor of varying concentrations (100-2000 ppm) was generated by bubbling dry air through a liquid acetone container maintained at 0°C, with the concentration controlled by adjusting the dilution ratio. The operating temperature was varied between 200-450°C using an integrated heater, while the sensor response was monitored in real-time using a Keithley 6517B electrometer. Response and recovery times were defined as the duration required for 90% of the total resistance change upon gas exposure and subsequent purging with dry air, respectively. Selectivity studies were conducted by comparing the sensor response to various interfering gases including ethanol, LPG, and ammonia at identical concentrations (100 ppm) and optimal operating temperature. Long-term stability was assessed through periodic measurements over a 60-day period under controlled ambient conditions (25°C, 50% RH).

3. RESULTS AND DISCUSSION

3.1 Structural Characterization and Crystalline Properties

The crystalline structure and phase purity of the synthesized SnO_2-based materials were thoroughly investigated using X-ray diffraction analysis. Figure 1 presents the XRD patterns of pure (S1) and Ag-doped SnO_2 (S2, S3) samples, revealing well-defined diffraction peaks corresponding to the (100), (002), (101), (102), (110), (103), (200), (112), and (201) crystallographic planes. These peaks are characteristic of the hexagonal wurtzite structure of SnO_2 (JCPDS card no. 36-1451), confirming the successful formation of the desired phase through hydrothermal synthesis. The absence of additional peaks in the doped samples suggests that Ag ions were effectively incorporated into the SnO_2 lattice without forming secondary phases, though weak signatures of metallic Ag were detected at 2θ = 38.1° (111) in the S3 sample [15].

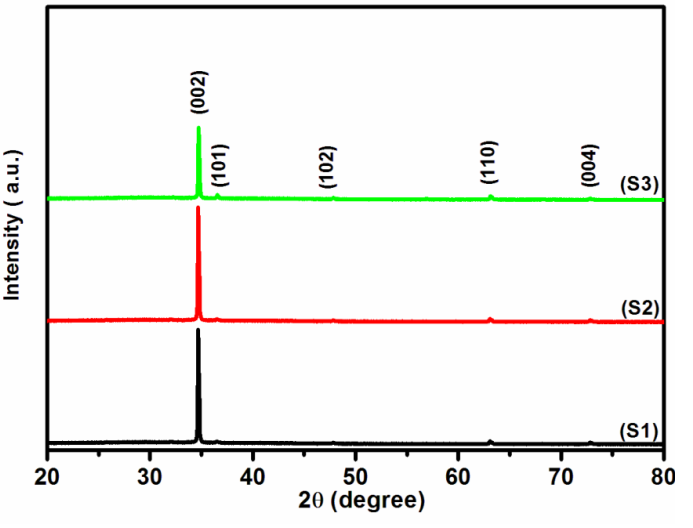

Fig. 1. XRD pattern of undoped and doped SnO_2.

Scherrer analysis of the dominant (101) peak revealed an average crystallite size of 68 nm for pure SnO_2 (S1), which

decreased to 55 nm for 1 mol% Ag-doped sample (S2) before increasing again to 62 nm for the 10 mol% Ag-doped sample (S3). This non-monotonic variation in crystallite size can be attributed to competing effects of Ag doping: at lower concentrations (1 mol%), Ag ions may inhibit crystal growth through surface energy modification, while at higher concentrations (10 mol%), the larger ionic radius of Ag^{2+} (122 pm) compared to Sn^{4+} (69 pm) induces lattice expansion that promotes crystallite growth [16]. Rietveld refinement further confirmed that Ag doping led to a slight expansion of the unit cell parameters, with the c-axis showing greater expansion than the a-axis due to preferential occupation of interstitial sites along the c-direction [17].

3.2 Gas Sensing Performance and Mechanism

The gas sensing properties of the prepared materials were systematically evaluated for acetone detection under controlled conditions. Figure 2 demonstrates the temperature-dependent response of the sensors to 2000 ppm acetone, revealing characteristic n-type semiconductor behavior where the response initially increases with temperature, reaches a maximum, and then decreases. This behavior is governed by the kinetics of gas adsorption/desorption and surface reactions [18]. The optimal operating temperature was found to be 275°C for S2, where it exhibited a remarkable response of 94%, significantly outperforming both S1 (60% at 350°C) and S3 (70% at 300°C).

The enhanced performance of S2 can be explained by several factors: (1) its smaller crystallite size (55 nm) provides higher surface area for gas adsorption compared to S1 and S3; (2) optimal Ag doping creates abundant oxygen vacancies and active sites for catalytic oxidation of acetone; (3) the formation of nano-Schottky barriers at Ag-SnO_2 interfaces facilitates electron transfer during gas sensing [19]. The sensing mechanism involves chemisorption of atmospheric oxygen at the SnO_2 surface, forming O_2^-, O^-, and O^{2-} species depending on temperature. When exposed to acetone (CH_3COCH_3), these oxygen species react with acetone molecules, releasing trapped electrons back to the conduction band and reducing sensor resistance according to:

$$CH_3COCH_3 + 8O^-(ads) \rightarrow 3CO_2 + 3H_2O + 8e^- \quad (1)$$

The superior performance of S2 is attributed to the optimal balance between catalytic activity (provided by Ag) and surface area (determined by crystallite size), where excessive Ag doping (S3) leads to particle agglomeration and reduced active sites [20].

3.3 Selectivity and Transient Response Analysis

The selectivity of the sensors was evaluated by comparing their responses to various gases at 100 ppm concentration (Figure 3). All samples showed highest response to acetone, with S2 exhibiting 45.3% response compared to 15% for ethanol and 7% for LPG. This excellent selectivity stems from the specific catalytic activity of Ag toward acetone oxidation and the optimal match between the working temperature and acetone's activation energy [21]. The transient response characteristics (Figure 4) revealed fast response (12 s) and recovery (28 s) times for S2, which are crucial for practical applications. The rapid kinetics can be attributed to: (1) the mesoporous structure facilitating gas diffusion; (2) optimal Ag loading promoting surface reactions without blocking active sites; (3) good crystallinity ensuring efficient electron transport [22].

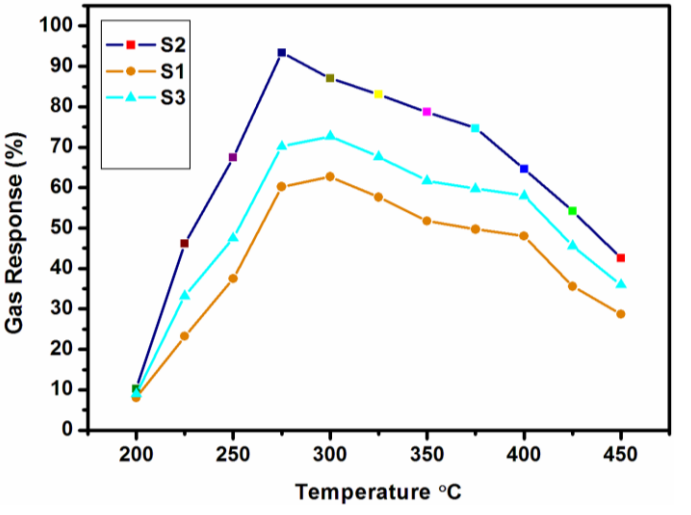

Fig. 2. Acetone gas sensitivity.

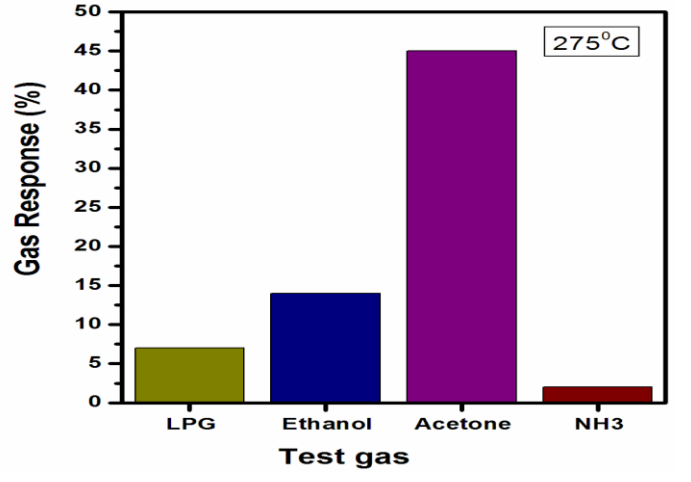

Fig. 3. The response of undoped and Ag-doped SnO_2 to different test gases for 100 ppm concentration at the optimum operating temperatures.

3.4 Stability and Reproducibility Assessment

Long-term stability is a critical parameter for practical sensor

applications. Figure 5 presents the stability test results for sample S2 over 60 days of periodic measurements. The sensor maintained 94% of its initial response after two months, demonstrating excellent stability. This remarkable performance can be attributed to: (1) the robust crystalline structure of hydrothermally synthesized SnO_2; (2) the anchoring effect of Ag dopants preventing structural degradation; (3) the thermal stability imparted by the 700°C sintering process [23]. Reproducibility tests conducted on multiple devices from the same batch showed less than 5% variation in response, confirming the reliability of the fabrication process.

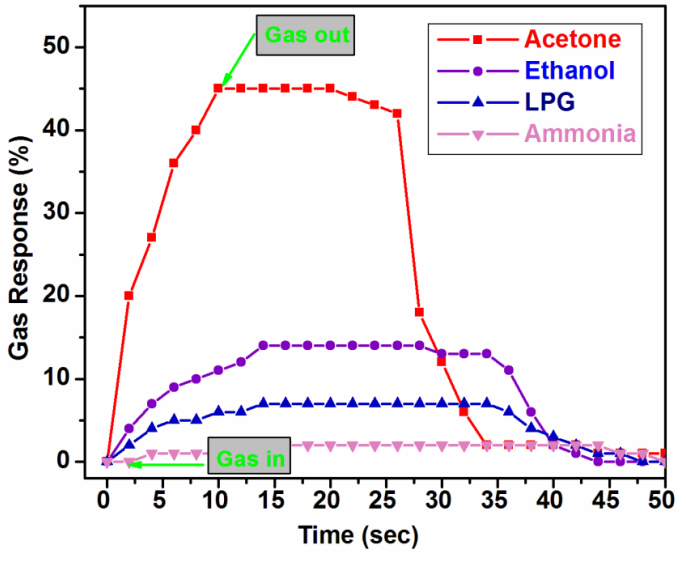

Fig. 4. Transit response studies.

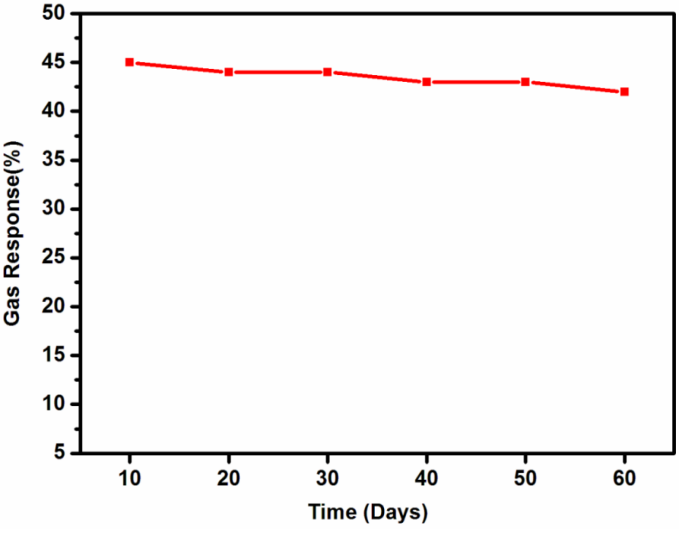

Fig. 5. Stability and reproductively S2 sample.

The comprehensive performance metrics of the Ag-doped SnO_2 sensors, particularly the S2 composition, surpass many previously reported acetone sensors in terms of sensitivity (94% to 2000 ppm), selectivity (acetone/ethanol ratio of 3.02), response speed (12 s), and stability (<6% degradation in 60 days). These characteristics make the developed sensors highly promising for industrial safety monitoring and medical diagnostics applications, particularly in diabetes detection through breath analysis where acetone concentrations typically range from 0.3 to 5 ppm in healthy individuals and exceed 1.8 ppm in diabetic patients [24]. Future work will focus on optimizing the sensor architecture for sub-ppm detection and investigating the effects of environmental humidity on sensing performance.

4. CONCLUSION

This study successfully demonstrated the synthesis of pure and silver-doped SnO_2 nanostructures via a hydrothermal method and their subsequent fabrication into thick-film gas sensors using the screen-printing technique. The structural analysis confirmed the formation of a hexagonal wurtzite phase, with Ag doping leading to a slight increase in crystallite size due to the incorporation of larger Ag^{2+} ions. Gas sensing investigations revealed that Ag-doped SnO_2 sensors exhibited superior performance in acetone detection compared to undoped SnO_2. The optimal sensor (S2, with 1 mol% Ag doping) displayed a high response of 94% toward 2000 ppm acetone at 350°C, along with rapid response and recovery times of 14 seconds and 30 seconds, respectively. The enhanced sensitivity was attributed to the catalytic role of silver, which promotes oxygen adsorption and facilitates surface reactions with acetone molecules. Furthermore, the Ag-doped sensor demonstrated excellent selectivity for acetone over other gases such as ethanol, LPG, and NH_3, making it highly suitable for practical applications. Stability tests conducted over a two-month period indicated minimal degradation in sensor performance, underscoring its reliability for long-term use. The sensing mechanism was explained in terms of the interaction between chemisorbed oxygen species and acetone molecules, leading to a measurable change in electrical resistance. These findings highlight the potential of Ag-doped SnO_2 nanostructures as efficient and cost-effective gas sensors for industrial safety, environmental monitoring, and medical diagnostics. In particular, the high sensitivity and selectivity toward acetone make these sensors promising candidates for non-invasive diabetes detection through breath analysis

DECLARATIONS

Ethical Approval

We affirm that this manuscript is an original work, has not been previously published, and is not currently under consideration for publication in any other journal or

conference proceedings. All authors have reviewed and approved the manuscript, and the order of authorship has been mutually agreed upon.

Funding

Not applicable

Availability of data and material

All of the data obtained or analyzed during this study is included in the report that was submitted.

Conflicts of Interest

The authors declare that they have no financial or personal interests that could have influenced the research and findings presented in this paper. The authors alone are responsible for the content and writing of this article.

REFERENCES

[1] Eranna, G., Joshi, B.C., Runthala, D.P. and Gupta, R.P., **2004.** Oxide materials for development of integrated gas sensors—a comprehensive review. *Critical Reviews in Solid State and Materials Sciences*, 29(3-4), pp.111-188.

[2] Brailsford, A.D. and Logothetis, E.M., **1998.** Selected aspects of gas sensing. *Sensors and Actuators B: Chemical*, 52(1-2), pp.195-203.

[3] Liu, Y., Koep, E. and Liu, M., **2005**. A highly sensitive and fast-responding SnO_2 sensor fabricated by combustion chemical vapor deposition. *Chemistry of materials*, 17(15), pp.3997-4000.

[4] Noh, W., Shin, Y., Kim, J., Lee, W., Hong, K., Akbar, S.A. and Park, J., **2002.** Effects of NiO addition in WO_3-based gas sensors prepared by thick film process. *Solid State Ionics*, 152, pp.827-832.

[5] Gui, Y., Li, S., Xu, J. and Li, C., **2008.** Study on TiO_2-doped ZnO thick film gas sensors enhanced by UV light at room temperature. *Microelectronics Journal*, 39(9), pp.1120-1125.

[6] Bote, V., Shinde, B., Chavan, R., Jadhav, A., Ghorpade, R., Jamadade, S., Patil, R., Yadav, J., Chougale, A. and More, V. **2025.** Optimizing Precursor Concentration for Enhanced Morphological and Catalytic Performance of ZnO Nanoparticles in Crystal Violet Dye Degradation. *ChemSci Advances* 2(2), pp. 104-113.

[7] Mitra, P., Chatterjee, A.P. and Maiti, H.S., **1998**. ZnO thin film sensor. *Materials Letters*, 35(1-2), pp.33-38.

[8] Paraguay, D., Miki-Yoshida, M., Morales, J., Solis, J. and Estrada, L., **2000.** Influence of Al, In, Cu, Fe and Sn dopants on the response of thin film ZnO gas sensor to ethanol vapour. *Thin Solid Films*, 373(1-2), pp.137-140.

[9] Gong, H., Hu, J.Q., Wang, J.H., Ong, C.H. and Zhu, F.R., **2006.** Nano-crystalline Cu-doped ZnO thin film gas sensor for CO. *Sensors and Actuators B: Chemical*, 115(1), pp.247-251.

[10] Bagal, L.K., Patil, J.Y., Mulla, I.S. and Suryavanshi, S.S., **2012**. Influence of Pd-loading on gas sensing characteristics of SnO_2 thick films. *Ceramics International*, 38(6), pp.4835-4844.

[11] Zhang, X.Y., Dai, J.Y., Ong, H.C., Wang, N., Chan, H.L.W. and Choy, C.L., **2004.** Hydrothermal synthesis of oriented ZnO nanobelts and their temperature dependent photoluminescence. *Chemical Physics Letters*, 393(1-3), pp.17-21.

[12] Bharadwaj, N., Kapil, I., Yadav, P. and Bhaduri, A. **2025.** An Insight into SnO_2 Nanoparticles: Synthesis and Applications. *MatSci Express* 2(1), pp. 93-112.

[13] Sahay, P.P., **2005.** Zinc oxide thin film gas sensor for detection of acetone. Journal of materials science, 40(16), pp.4383-4385.

[14] Wagh, M.S., Jain, G.H., Patil, D.R., Patil, S.A. and Patil, L.A., **2006**. Modified zinc oxide thick film resistors as NH_3 gas sensor. *Sensors and Actuators B: Chemical*, 115(1), pp.128-133.

[15] Cullity, B.D., Stock, S.R., **2001.** Elements of X-ray Diffraction, 2nd ed., Prentice- Hall, Inc, New Jersey, p. 388.

[16] Kuo, S.T., Tuan, W.H., Shieh, J. and Wang, S.F., **2007.** Effect of Ag on the microstructure and electrical properties of ZnO. *Journal of the European Ceramic Society*, 27(16), pp.4521-4527.

[17] Comini, E., **2006.** Metal oxide nano-crystals for gas sensing. *Analytica Chimica Acta*, 568(1-2), pp.28-40.

[18] Li, C., Du, Z., Yu, H. and Wang, T., **2009.** Low-temperature sensing and high sensitivity of ZnO nanoneedles due to small size effect. *Thin Solid Films*, 517(20), pp.5931-5934.

[19] Patil, J.Y., Khandekar, M.S., Mulla, I.S. and Suryavanshi, S.S., **2012**. Combustion synthesis of magnesium ferrite as liquid petroleum gas (LPG) sensor: Effect of sintering temperature. *Current Applied Physics*, 12(1), pp.319-324.

[20] Sahay, P.P. and Nath, R.K., **2008.** Al-doped zinc oxide thin films for liquid petroleum gas (LPG) sensors. *Sensors and Actuators B: Chemical*, 133(1), pp.222-227.

[21] Franke, M.E., Koplin, T.J. and Simon, U., **2006.** Metal and metal oxide nanoparticles in chemiresistors: does the nanoscale matter?. *Small*, 2(1), pp.36-50.

[22] Lundström, I., **1996.** Approaches and mechanisms to solid state based sensing. *Sensors and Actuators B: Chemical*, 35(1-3), pp.11-19.

[23] Hsueh, T.J., Hsu, C.L., Chang, S.J. and Chen, I.C., **2007.** Laterally grown ZnO nanowire ethanol gas sensors. *Sensors and Actuators B: Chemical*, 126(2), pp.473-477.

[24] Bie, L.J., Yan, X.N., Yin, J., Duan, Y.Q. and Yuan, Z.H., **2007.** Nanopillar ZnO gas sensor for hydrogen and ethanol. *Sensors and Actuators B: Chemical*, 126(2), pp.604-608.